

# An Alfvén wave maser in the laboratory

J. E. Maggs, G. J. Morales, and T. A. Carter

*Physics and Astronomy Department, University of California, Los Angeles, California 90095*

(Received 22 June 2004; accepted 28 September 2004; published online 14 December 2004)

A frequency selective Alfvén wave resonator results from the application of a locally nonuniform magnetic field to a plasma source region between the cathode and anode in a large laboratory device. When a threshold in the plasma discharge current is exceeded, selective amplification produces a highly coherent ( $\delta\omega/\omega < 5 \times 10^{-3}$ ), large amplitude shear Alfvén wave that propagates out of the resonator, through a semitransparent mesh anode, into the adjacent plasma column where the magnetic field is uniform. This phenomenon is similar to that encountered in the operation of masers/lasers at microwave and optical frequencies. The current threshold for maser action is found to depend upon the confinement magnetic field strength  $B_0$ . Its scaling is consistent with the condition for matching the drift speed of the bulk plasma electrons with the phase velocity of the mode in the resonator. The largest spontaneously amplified signals are obtained at low  $B_0$  and large plasma currents. The magnetic fluctuations  $\delta B$  associated with the Alfvén maser can be as large as  $\delta B/B_0 \approx 1.5\%$  and are observed to affect the plasma current. Steady-state behavior leading to coherent signals lasting until the discharge is terminated can be achieved when the growth conditions are well-above threshold. The maser is observed to evolve in time from an initial  $m=0$  mode to an  $m=1$  mode structure in the transition to the late steady state. The laboratory phenomenon reported is analogous to the Alfvén wave maser proposed to exist in naturally occurring, near-earth plasmas. © 2005 American Institute of Physics. [DOI: 10.1063/1.1823413]

## I. INTRODUCTION

The coherent amplification of electromagnetic radiation leading to laser or maser action requires that a combination of essential physical processes be brought together in a compatible geometrical arrangement. These include an active medium where a nonequilibrium population is maintained. Its role is to selectively amplify the electromagnetic wave over a narrow frequency interval. Another essential element is a partial reflector which plays a dual role. It allows the spontaneously amplified signal to undergo multiple passes through the active medium, while simultaneously allowing the final, large amplitude beam to exit into the region of interest. In working with optical or microwave frequencies the requirements are satisfied by judicious choices of atomic species driven to exhibit inverted populations within a cavity bounded by suitable mirrors. In the present study a laboratory realization of an analogous situation is reported, but involving shear Alfvén waves.

Theoretical studies<sup>1-3</sup> have investigated the concept of a natural Alfvén wave maser formed in the plasmas surrounding the earth. Some theories consider the maser cavity formed by the magnetospheric plasma bounded by the highly conducting, conjugate ionospheres. These relatively narrow regions play the role of reflectors. The nonequilibrium, active material has been associated with a population of energetic ions<sup>1</sup> in the radiation belt. Another class of Alfvén maser activity is considered to occur at the lower altitudes. Due to the spatial variation of the ionospheric plasma parameters, it has been identified in various studies<sup>4-7</sup> that an Alfvén resonator is naturally formed between the lower  $E$  region of the ionosphere and a region in the topside ionosphere at an altitude of about  $10^4$  km. This higher region acts as a partial

reflector that allows amplified signals to propagate into the magnetosphere. Recent observations by satellite<sup>8</sup> and rocket<sup>9</sup> suggest that signals consistent with resonant amplification of Alfvén waves are naturally generated and corroborate ground-based measurements<sup>10,11</sup> of the phenomena. The amplified signals correspond to waves that undergo multiple reflections within the resonator. A recent modeling study<sup>12</sup> has proposed that the strong fluctuations associated with the partially standing waves in the ionospheric resonator are responsible for driving the outflow of source ions from the ionosphere to fuel the magnetospheric plasma.

Various nonequilibrium sources have been considered to excite the ionospheric Alfvén resonator. These include the natural magnetospheric convection,<sup>4,13</sup> electron beams,<sup>14</sup> lightning discharges,<sup>15,16</sup> and powerful HF radio signals.<sup>17</sup> In the present laboratory study an equivalent Alfvén resonator is realized in which the nonequilibrium source leading to spontaneous amplification is a field-aligned current.

The present paper provides detailed experimental information about the operation of an Alfvén-wave maser under controlled conditions in a large laboratory plasma device. For a shorter description of the highlights the reader is referred to the original publication<sup>18</sup> reporting the first discovery of this phenomenon. A useful wider perspective on this topic can also be gained from the review by Boswell.<sup>19</sup>

The paper is organized as follows. Section II A describes the properties of the plasma device used, Sec. II B explains the unique features of the resonant cavity, and Sec. II C outlines the ambient current system that provides the free energy source for the maser. Section III A introduces the spontaneous magnetic fluctuations below threshold. Section III B presents the near-threshold behavior while Sec. III C illus-

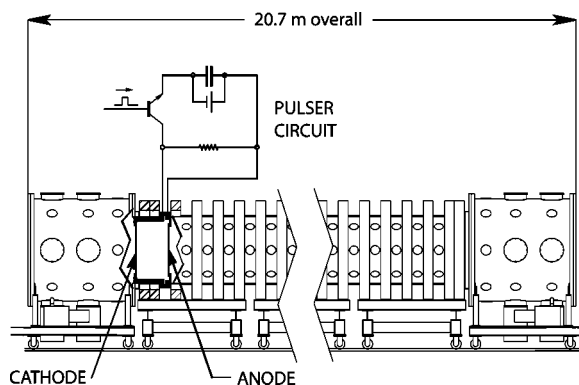


FIG. 1. A truncated schematic of the LAPD-U showing some of the vacuum chamber, a cutaway of the cathode-anode region where maser action occurs, and the discharge pulser circuit.

trates maser behavior well-above threshold. Section IV examines mode transitions and Sec. V gives examples of nonlinear phenomena. Discussions are presented in Sec. VI.

## II. EXPERIMENTAL ARRANGEMENT

### A. Properties of the plasma device

The experimental results reported here are obtained in plasmas generated in the upgraded large plasma device (LAPD-U) operated by the Basic Plasma Science Facility at the University of California, Los Angeles. A schematic of the device is shown in Fig. 1. The LAPD-U vacuum chamber is 21 meters in overall length. Two end-bells (1.5 m diameter, 2 m long) house the turbo-molecular vacuum pumps. The plasma section of the device where wave properties are routinely measured is a 1 m diameter vacuum vessel surrounded by water-cooled magnetic coils that provide the radial plasma confinement. The coils are divided into ten groups powered by separate, regulated dc supplies that are computer controlled. Presently this configuration permits practical operation of plasma conditions over the range of 300–2000 G. This arrangement also allows for a wide variety of confinement magnetic-field profiles (e.g., local mirrors or cusps). For the maser studies reported here the confinement magnetic field is of uniform strength within the magnetic solenoid having a total length of 17.5 m. The plasma is produced by a hot-cathode source located at one end of the main magnetized plasma column. The cathode is a pure Nickel sheet coated with a thin layer of barium oxide heated to emission temperature of about 800 °C. The anode is a Molybdenum mesh ( $\approx 50\%$  transparent) located a distance of 55 cm from the cathode. This source is used to create a beam of electrons of typical energy in the 50 eV range and carrying currents of 3–6 kA. The energetic electrons (i.e., primaries) that pass through the mesh anode ionize an initial column of neutral He gas (at a fill pressure of  $1 \times 10^{-4}$ – $2 \times 10^{-4}$  Torr) in the uniformly magnetized section of the machine. Under steady conditions He plasmas having densities in the range of  $1 \times 10^{12}$ – $3 \times 10^{12}$  cm $^{-3}$  are generated with greater than 50% degree of ionization. The characteristic electron temperature is 6–8 eV with the ion temperature in the range of 1 eV.

In the present study the plasma device is operated with a floating end chamber. This implies that there is no net current collected at the far end of the machine. Since a current is continuously injected through the fast primary electrons this implies that the bulk plasma electrons develop a self-consistent drift  $v_D$  in the direction pointing towards the anode. It is this drift velocity that can resonate with shear Alfvén waves; the primary electrons move much faster than the Alfvén speed  $v_A$ .

### B. Features of the maser cavity

Since shear Alfvén waves propagate primarily along the confinement magnetic field, partially standing shear waves can be created by reflection from boundaries with normals oriented along the axial direction. Standing shear waves undergoing reflections between two such boundaries can thus become cavity resonances when driven by a source of energy. An effective resonant cavity for shear Alfvén waves is provided in the LAPD-U plasma-source region by the solid Nickel cathode and the partially transparent Molybdenum mesh anode 55 cm away. The transparency of the mesh anode is, of course, necessary to allow fast, ionizing electrons to enter the main chamber and form a plasma. The semitransparent mesh anode also allows wave energy in the resonant cavity to escape along field lines into the main plasma column where the routine wave-propagation studies are performed.

A key feature of the resonant cavity in the LAPD-U is the spatial dependence of the confinement magnetic field in this region. Since the cathode-anode combination is located near the end of the magnetic solenoid, the end magnets are uncompensated on one side and this naturally results in the confinement magnetic field flaring in the region between the anode and cathode. A schematic of this situation is shown in Fig. 2(a). The flaring field leads to a decrease in the magnetic field strength in the resonant cavity as illustrated in Fig. 2(b). For the case of a uniform confinement magnetic field in the main plasma column, the magnetic field strength in the resonant cavity decreases from 95% of the column magnetic field at the anode to 65% at the cathode. The decreasing magnetic field strength in the cavity has important consequences for the maser production process: it changes the parallel wavelength of the waves, broadens the range of wave phase velocities, and limits the number of modes supported within the resonant cavity. Analogous features are also encountered in the ionospheric Alfvén resonator in which the spatial variation of the wave properties results from the variation of the ionospheric plasma parameters with distance from the earth's surface.

The spatially varying magnetic field in the cathode-anode region leads to local changes in the parallel wavelength of the propagating shear waves. In the regime of interest here in which the Alfvén speed is less than the electron thermal velocity, the parallel wavelength,  $\lambda(f, z)$  of a shear wave propagating with frequency  $f$  along the magnetic field in the  $z$  direction is approximately given by

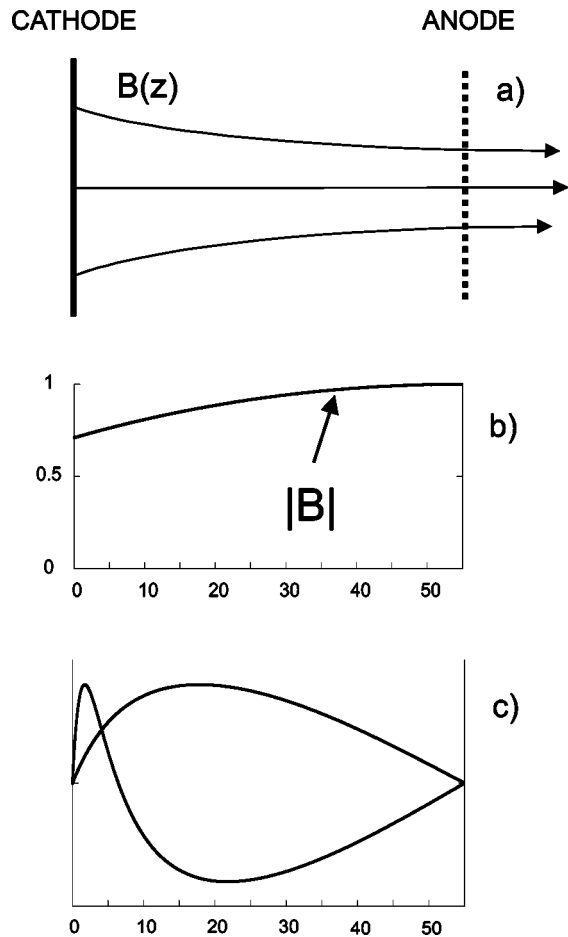


FIG. 2. (a) Schematic indicating that the magnetic field lines in the LAPD-U flare out in the region between the anode and cathode. (b) Decreasing magnetic field strength within the resulting resonant cavity. (c) The WKB waveforms for the first two modes of the resonant cavity.

$$\lambda(f, z) = \frac{V_A(z)}{f} \left\{ 1 - \left( \frac{f}{f_{ci}(z)} \right)^2 + [k_{\perp} \rho_s(z)]^2 \right\}^{1/2}, \quad (1)$$

where  $V_A(z) = B(z)/(4\pi nM)^{1/2}$  is the Alfvén speed for a plasma of density  $n$  and ion mass  $M$ ,  $f_{ci}(z)$  is the ion cyclotron frequency at axial location  $z$ ,  $k_{\perp}$  is the perpendicular wave number, and  $\rho_s(z)$  is the ion sound gyroradius,  $c_s/[2\pi f_{ci}(z)]$ . Thus, as a wave propagates in the direction of decreasing magnetic field, the wavelength decreases both because the Alfvén speed decreases and because the frequency is approaching the local ion cyclotron frequency.

For illustrative purposes, assume the normalized electric field of standing waves in the resonant cavity has an approximate Wentzel–Kramers–Brillouin (WKB) form. Standing, or resonant, modes occur approximately at those frequencies for which an integer multiple of a half-wavelength fits between the anode and cathode. The WKB-model electric field of the first two resonant modes is shown in Fig. 2(c). Notice that the wavelength changes rapidly in the vicinity of the cathode. The shortening of the wavelength allows for the possibility of fitting a half-wavelength of an Alfvén wave into a cavity at a frequency lower than would be needed if the field were uniform. Also, the changing wavelength leads

to a changing wave phase velocity, so that, in the resonant cavity, the wave phase velocity sweeps over an extended range in velocity space.

In principle, a large number of resonant modes can fit into the resonant cavity, particularly for short wavelength shear modes corresponding to frequencies slightly below the ion cyclotron frequency. However, the changing magnetic field profile results in a drastic reduction in the number of viable resonant modes, i.e., it provides an effective low pass filter. This reduction arises from selective absorption of energy as the fixed frequency of a mode matches the local ion cyclotron frequency. Shear modes are left-hand polarized and thus strongly damped at the ion cyclotron frequency, and evanescent for frequencies above it. In practice, only the lowest frequency, resonant mode is significantly enhanced in the cavity. An important consequence of this geometrical selectivity is that the frequency of this lowest mode, which is a candidate for maser action, is a fixed numerical fraction of the ion cyclotron frequency in the uniform section of the downstream plasma column where the wave properties are sampled. This implies that under suitable amplification conditions it is possible to select the frequency of the operating maser by simply changing the strength of the magnetic field, i.e., one achieves a continuously tunable source of coherent shear Alfvén waves.

### C. Free energy source

To ascertain that a bulk electron drift velocity is present in the plasma, the signals sampled by a double-sided Langmuir probe are examined. In principle, this drift can provide the free energy to amplify the modes supported in the resonator cavity previously described and thus result in maser action.

The probe used is double sided (such as a Mach probe) and a voltage ramp is simultaneously applied to both faces. The probe faces are planar and the probe is oriented with each face perpendicular to the direction of the confinement magnetic field. One face points directly toward the cathode and the other away. At a given applied voltage the difference in the current (i.e., electron flux) to each face indicates the total current carried by electrons of energy equal or greater than the applied voltage (relative to plasma potential). At plasma potential, the difference is a measure of the total field-aligned current on the flux tube threading the probe.

The top panel in Fig. 3 shows two Langmuir probe traces as a function of energy relative to the plasma potential energy  $E_p$  in units of the kinetic energy of an electron traveling at the Alfvén speed  $E_A$ . The bottom panel shows the difference between the two current traces as a function of velocity in units of the Alfvén speed. The probe is located in the main plasma column at a radial position near the column center and an axial distance 2.2 m from the semitransparent anode. The strength of the confinement field is 600 G, which (as is shown later) corresponds to a situation when maser action is present.

The top panel of Fig. 3 clearly shows the current carried by the degraded primary electrons. The face looking away from the cathode shows a Maxwellian distribution of elec-

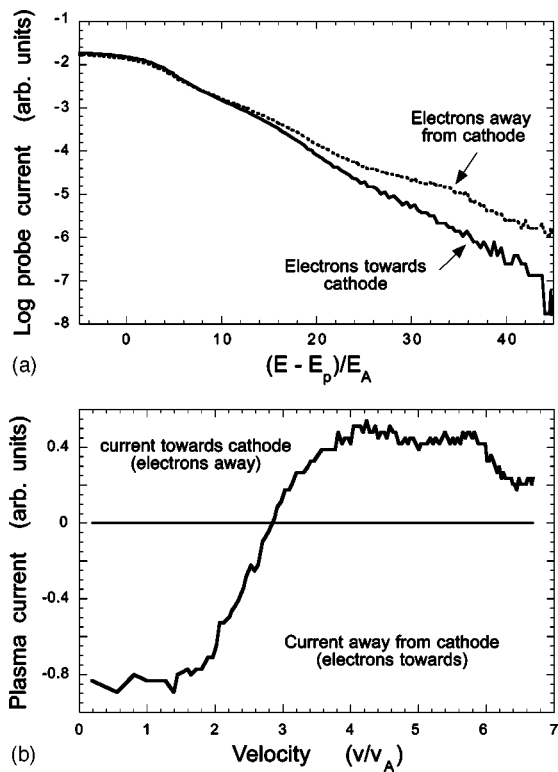


FIG. 3. (a) Two Langmuir-probe current vs voltage traces in which the voltage is referenced to the plasma potential  $E_p$  and normalized to the electron Alfvén kinetic energy  $E_A$ . The traces are obtained simultaneously from a double-sided probe located in the main plasma column 2.2 m from the anode. The probe is oriented so that one side samples field-aligned electron flux away from the cathode and the other side samples flux towards the cathode. (b) The difference between the two probe traces as a function of electron velocity normalized to the Alfvén speed. At a given velocity, this difference is a measure of the current carried by particles with greater or equal velocity.

trons for energies below plasma potential. This is evident because the probe trace is very nearly linear, and a Maxwellian distribution would appear as a straight line in this semi-log plot. On the other hand, the face looking towards the cathode shows clear evidence of a non-Maxwellian tail for the faster electrons. These faster electrons are the primary electrons injected at the cathode but degraded in energy due to ionizing collisions. Since, for higher energies (i.e., more negative bias voltages), the flux to the face looking towards the cathode exceeds the flux to the face looking away, it is clear that the primary electrons constitute a current flowing towards the cathode. The bottom panel of Fig. 3 shows that the current decreases, and in this particular case even reverses sign, as the voltage on the probe approaches plasma potential. The current changes sign because the main plasma electrons are carrying a current in the direction opposite the current carried by the fast electrons. Indeed, for this particular field line, a total current is flowing in the direction opposite the discharge electron current. This fact is indicated by the negative value of the current in the bottom panel of Fig. 3 at a value of zero velocity (the velocity is zero for electrons at plasma potential). It is to be noted that this is a local result pertaining to a small bundle of field lines. On average across the entire plasma column, the total field-aligned cur-

rent (i.e., the current at plasma potential) is zero. An electron velocity distribution function consistent with these probe measurements is a bulk Maxwellian with a drift velocity towards the cathode of a few tenths the electron thermal speed plus a fast tail moving away from the cathode.

The measurements presented in Fig. 3 are obtained in the main plasma column and not the resonator region. However, since the anode is 50% transparent, half of the Maxwellian electrons drifting toward the anode would pass into the cathode-anode region, so it is expected that a return current is present within the maser cavity. The return current can directly interact with and amplify the resonant shear Alfvén wave. Amplification occurs if the local wave phase velocity is in a region of velocity space where the distribution function exhibits a positive slope. For the drifting-Maxwellian model, this requires that the drift speed of the bulk electrons exceed the wave phase velocity. Thus, for growth, the wave phase velocity must be on the order of a few tenths of the electron thermal velocity. Due to the decreasing magnetic field strength in the source region, the wave phase velocity in the source is much lower than in the main plasma column, so that the electrons undergoing wave-particle interactions are those with velocities below the Alfvén speed in the main plasma column, i.e., corresponding to velocities less than unity in the bottom panel of Fig. 3.

### III. SPONTANEOUS MAGNETIC FLUCTUATIONS

#### A. Behavior in the absence of maser action

The plasma between the anode and cathode provides a source of spontaneous shear Alfvén wave noise. Waves excited in the source region pass through the mesh anode and propagate into the main plasma column where they can be easily detected and also where the magnetic field is uniform. The fluctuating wave fields are typically measured at an axial location near the middle of the plasma column using a tri-axial induction loop probe ( $B$ -dot probe) which measures the time derivative of the wave magnetic vector. Figure 4 displays the log of the power spectrum of the transverse component of the magnetic noise observed in the plasma column in the absence of maser action. It should be noted that the frequency is scaled to the value of the ion cyclotron frequency corresponding to the uniform magnetic field where the measurement is made. Since the observed axial component of the fluctuations is negligible compared to their transverse component, and their frequency is below the ion cyclotron frequency, the spontaneous fluctuations are identified as shear Alfvén waves.

The operating conditions leading to Fig. 4 correspond to a uniform magnetic field of 1000 G and discharge current of 5000 kA. The spectrum is seen to be broadband and can be classified by the three regions indicated in Fig. 4. The lower end extending to the lowest measured frequencies (about 35 kHz) corresponds to long-wavelength, nonresonant modes. Close to a frequency of  $0.6f_{ci}$  there is a rising peak associated with the lowest resonant mode supported by the cavity. At higher frequencies the noise drops precipitously due to damping as cyclotron resonance is approached somewhere within the cavity for these short wavelength modes. It

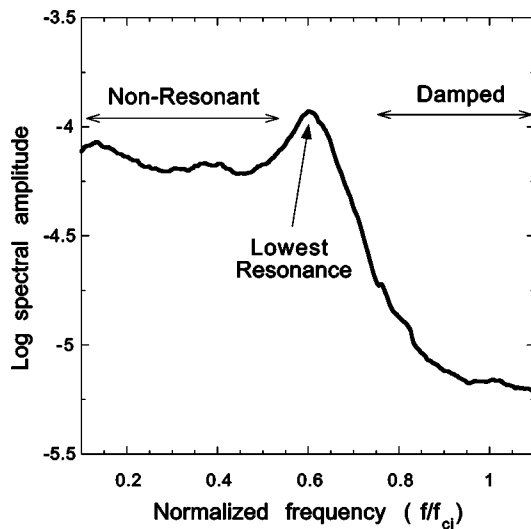


FIG. 4. The spectral amplitude (log scale) of the  $x$  component of the fluctuating magnetic field measured in the center of the main plasma column at distance  $z=4.9$  m from cathode for  $B_0=1000$  G, below maser threshold. The peak in the spectrum at  $0.6f_{ci}$  corresponds to the lowest resonant mode and becomes the maser mode above threshold. Note the sharp decrease in ambient noise above  $0.7f_{ci}$ .

should also be emphasized that the shape of the noise spectrum shown in Fig. 4 has been demonstrated in a previous study [Fig. 5 of Ref. 20] to be universal, i.e., the features are found to remain the same as the strength of the magnetic field is varied from 700 to 1300 G for discharge currents below a threshold value. In particular, the peak seen before the rapid decrease in amplitude in Fig. 4 always appears at  $0.6f_{ci}$ .

Confirmation that the plasma in the anode-cathode region is the actual source of the ambient noise observed in the main plasma column (and having the shape shown in Fig. 4) is obtained by measuring the axial evolution of the observed noise in a linearly decreasing axial magnetic field within the main plasma column, and has been previously reported (Fig. 10 of Ref. 20). Further evidence is provided by independently changing the strength of the magnetic field in the source region while holding the magnetic field constant in the main plasma column. Under such variation it is found that the gap between the highest shear-wave frequency and the ion cyclotron frequency (i.e., the region between  $0.65f_{ci}$  and  $f_{ci}$  in Fig. 4) tracks the field between the cathode and the anode and not the field in the main plasma column.

To obtain deeper insight into the significance of the peculiar universal shape of the ambient noise spectrum, a simple mathematical model of the frequency behavior of an Alfvén resonator is used. The model considers two regions with spatially uniform parameters but each having different values. The two regions are separated by a boundary (the anode) having a wave reflection coefficient  $R_A$ . The strength of the magnetic field in the source region [illustrated in Fig. 2(b)] is taken as the average value between the anode and the cathode locations. The scaled fluctuating field amplitude  $\psi$ , at axial position  $z$  within the plasma column, and at angular frequency  $\omega$  excited by a white-noise source is given by

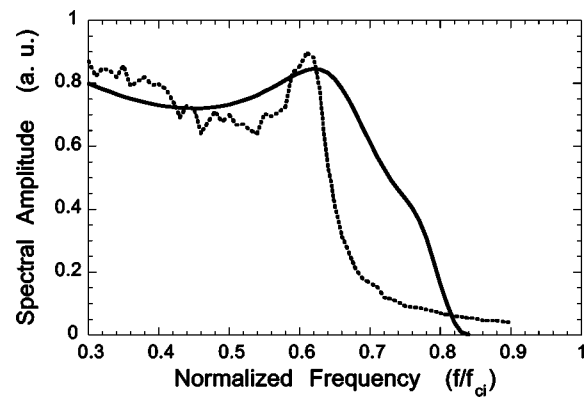


FIG. 5. Comparison of the prediction of a model consisting of partial wave reflections between cathode and anode (solid curve) and the measured ambient noise (broken curve) frequency spectrum in linear scale. The peak near  $0.6f_{ci}$  corresponds to the theoretically predicted first resonant mode within the cathode-anode cavity. The quenching at higher frequencies results from the nonuniform magnetic field in the cavity.

$$\psi(z, \omega) = \exp\{i[k_r(\omega)L + k_p(\omega)z]\} / \{1 - R_A \exp[i2k_r(\omega)L]\}, \quad (2)$$

where  $L$  is the distance between the cathode and the anode. The wave numbers in the main plasma column and in the resonator region are  $k_p$  and  $k_r$ , respectively. These wave numbers are calculated from the shear wave dispersion relation,

$$k_{\parallel}^2 \epsilon_{\parallel} + k_{\perp}^2 \epsilon_{\perp} = k_0^2 \epsilon_{\parallel} \epsilon_{\perp}, \quad (3)$$

in which the effects of electron-ion Coulomb collisions<sup>21</sup> and ion-neutral collisions<sup>22</sup> are included in the evaluation of the dielectric coefficients  $\epsilon_{\parallel}$  and  $\epsilon_{\perp}$ . The transverse wave number is  $k_{\perp} = \pi/a$ , where  $a$  is the plasma radius and  $k_0 = \omega/c$  with  $c$  the speed of light. The prediction of Eq. (2) for characteristic plasma parameters in the source and column regions is shown as the solid curve in Fig. 5, representing  $|\psi|$ . The broken curve corresponds to the experimentally observed spectrum, displayed in linear scale. It can be seen that the general features observed are reproduced by this simple model of the resonator. There is a low-frequency broadband region terminating in a local peak at  $0.6f_{ci}$  and a gap that appears well below  $f_{ci}$ . However, the drop in amplitude beyond the peak is not as abrupt as is observed in the experiment. The discrepancy of the model in this higher-frequency interval indicates that the continuously varying magnetic field produces a stronger damping of the waves than is estimated by a locally uniform model. Aside from showing the consistency between a resonator model and the experimental observations, what is of significance in Fig. 4 is that the universal peak at  $0.6f_{ci}$  corresponds mathematically to the first resonant mode supported by the resonator. It is this mode that is the prime candidate for maser behavior if a source of free energy is made available that can lead to its amplification. In the present configuration the plasma current provides such a source when its value exceeds a threshold level.

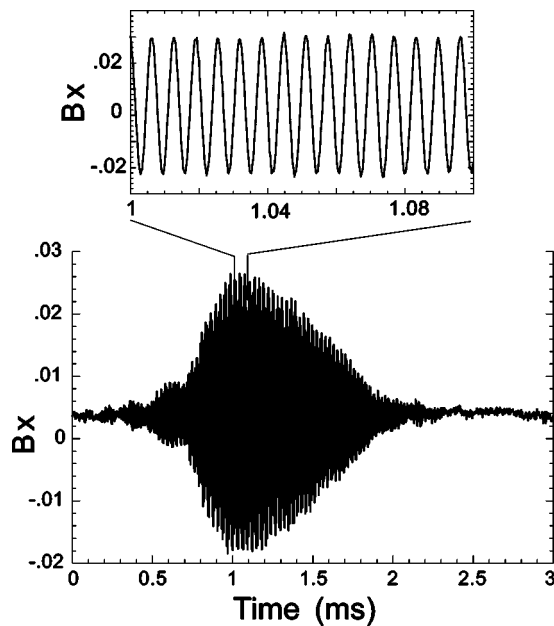


FIG. 6. Bottom panel: single-shot temporal evolution of the horizontal component of magnetic field for conditions near maser threshold measured at center of plasma column 8.75 m from cathode,  $B_0=700$  G. Top panel: expanded temporal behavior showing high degree of coherency for signal growing from spontaneous noise.

## B. Behavior close to maser threshold

The bottom panel of Fig. 6 shows the temporal behavior of the spontaneous magnetic fluctuations obtained when the plasma current just exceeds a threshold level (about 3.5 kA) for a confinement magnetic field of 700 G. The measurement is performed at a radial position near the center of the main plasma column and the quantity displayed is the horizontal component, or “x component,” of the wave field. As in the broadband spontaneous noise observed below threshold, the wave magnetic field is perpendicular to the background axial magnetic field; no field-aligned component is detectable. Again, this is the behavior expected for a shear Alfvén wave. For this case, which is representative of the behavior near threshold, the wave magnetic field flares, i.e., it grows rapidly, reaches a value of about one percent of the confinement magnetic field and then decays. It should be noted that the envelope of the actual flare signal is smooth, and not jagged as it appears in the bottom panel of Fig. 6 due to under sampling of the original time trace used in producing the figure.

The top panel of Fig. 6 displays an expanded view of the temporal behavior (single shot) of the flare event over a small interval of 0.1 msec. It shows that the flaring shear mode is nearly monochromatic and remarkably coherent, in particular since it grows out of spontaneous ambient noise. Detailed examination of the signal indicates, however, that the frequency of the wave slowly changes throughout the flare, decreasing about three percent from its initial value of 160 kHz or  $0.6f_{ci}$ , which corresponds to the resonant mode of the cathode-anode resonator identified previously in Figs.

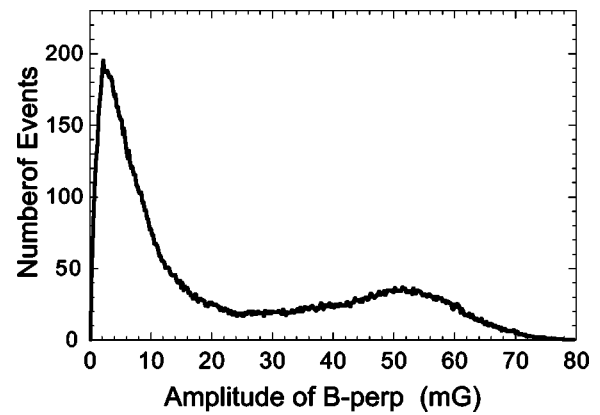


FIG. 7. Statistical properties of flaring maser fluctuations for near-threshold conditions. Low amplitude component has a Gaussian distribution while bump-on-tail corresponds to the coherent signals at  $0.6f_{ci}$ .

4 and 5. The change in frequency of the flaring resonant mode is most likely due to the changing plasma parameters as the plasma discharge evolves.

Near threshold the behavior of the spontaneous magnetic fluctuations can consist of multiple flare-events as the changing parameters bring the resonant cavity mode in and out of the zone where the free energy source can be tapped. The statistics of the ensuing behavior is exhibited in Fig. 7. It is seen that the probability distribution function consists of two components: a core having small amplitudes and a “bump-on-tail” at large amplitudes. The core component can be accurately fit by a Gaussian distribution and corresponds to the typical, below-threshold behavior associated with the spectrum of Fig. 4. The non-Gaussian component corresponds to the highly coherent events exemplified by Fig. 6.

The thick solid curve found in the three panels in Fig. 8 shows the measured variation in the threshold plasma current with the strength of the confinement magnetic field corresponding to the uniform plasma column. For a fixed value of the confinement magnetic field the maser is active for discharge currents higher than the threshold current at that field strength. The dotted lines on either side of the solid line in Fig. 8 indicate the uncertainty in determining the threshold. The three panels in Fig. 8 correspond to the same data but are used to illustrate the sensitivity of a model prediction represented by the thin straight lines. The model associates the growth of the spontaneous fluctuations with a wave-particle resonance between the resonant cavity mode and the drift velocity  $v_D$  of the bulk, background electrons. This drift arises in the plasma, without external experimental control, in order to cancel the current injected into the main plasma column by the fast, primary electrons (i.e., half the total discharge current), as documented in Sec. II C. The condition for wave-particle resonance can be translated into a threshold value  $I_t$  for the discharge current, namely,  $I_t = f \lambda n e \pi a_c^2$ , where  $f$  is the mode frequency having wavelength  $\lambda$  given by Eq. (1),  $n$  is the background plasma density,  $e$  the quantum of charge, and  $a_c$  corresponds to the effective radius of the region that carries the return current within the plasma. The model curves shown in Fig. 8 are calculated assuming that the threshold value of the current is attained for the mini-

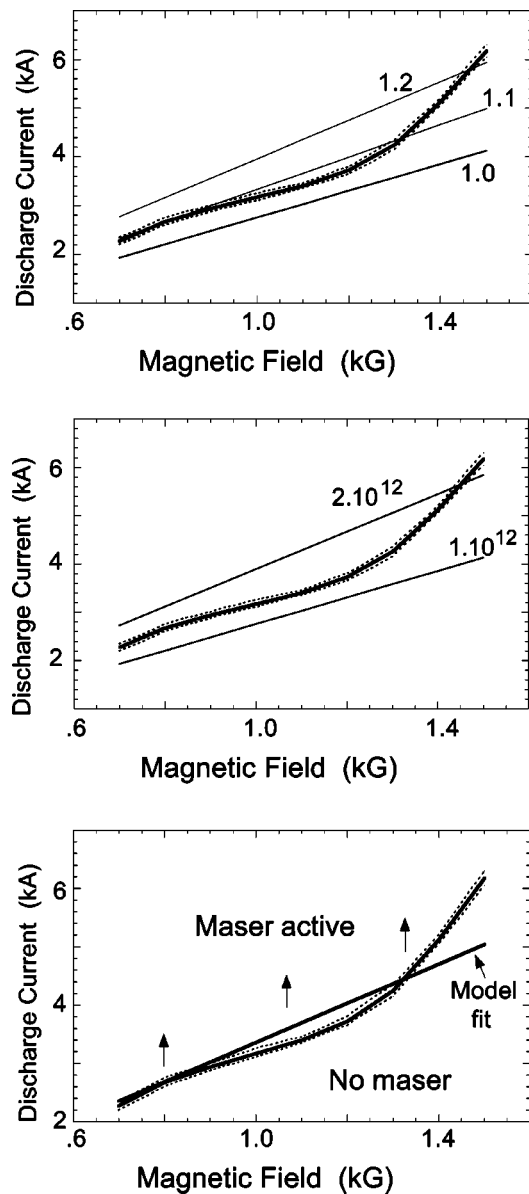


FIG. 8. Threshold parameter space for maser action. At fixed confinement field the discharge current must be larger than the value indicated by the thick curve in order for signals such as in Fig. 6 to appear. The three panels show the same data but test the sensitivity of model fits (thin straight lines) based on resonant condition that smallest wave phase velocity matches the bulk electron drift. Top panel shows sensitivity to effective radius of return current for fixed density. Middle panel shows sensitivity to average plasma density for fixed current radius. Bottom panel shows best parameter fit of model to data.

imum phase velocity in the source region. The top panel exhibits the sensitivity to the value of  $a_c$  for a fixed density of  $n=1 \times 10^{12} \text{ cm}^{-3}$ . The curve labeled “1.0” corresponds to  $a_c=7.0 \text{ cm}$ , while the other curves are 1.1 and 1.2 times this value as marked. The middle panel shows the sensitivity to the value of the density  $n$  for a fixed  $a_c=7.0 \text{ cm}$ . Finally, the bottom panel shows a model fit to the data using  $a_c=7.0 \text{ cm}$  and  $n=1.5 \times 10^{12} \text{ cm}^{-3}$ .

It is seen from the comparison between the model and the experimentally observed threshold that it is quite likely that the threshold for maser action is determined by the wave-particle resonance condition  $v_D=f\lambda(f)$  with  $f$  corre-

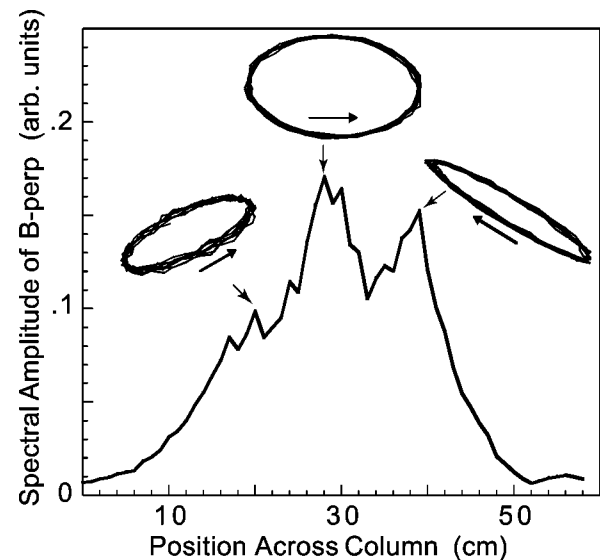


FIG. 9. Spatial pattern of maser action exhibits global mode. Lower curve is the dependence of the spectral amplitude of the transverse component of the magnetic fluctuations on the horizontal position across the main plasma column (plasma center is at 32 cm). The hodograms on top of the curve show the transverse polarization at the various positions.

sponding to the frequency of the resonant cavity mode, i.e.,  $f=0.6f_{ci}$ . The deviations from the scaling seen as  $B_0$  increases can be attributed to relatively small variations in the plasma parameters. Some of these variations are due to the time evolution of the plasma discharge and others are due to the intrinsic dependence of the plasma discharge on the strength of the confinement field.

The spatial profile of the flaring maser mode illustrated in Fig. 6 is shown in Fig. 9. This figure displays the amplitude of the transverse magnetic fluctuations, i.e.,  $[(\delta B_x)^2 + (\delta B_y)^2]^{1/2}$  along a horizontal cut across the plasma column at an axial distance  $z=8.75 \text{ m}$  from the cathode. It is seen that the maser signal is a global mode across the column. From correlation measurements between a probe inserted in the cathode-anode region and another in the main plasma column it is deduced also that the mode is global in the axial direction. The polarization properties of the maser signal are shown by the hodograms in Fig. 9 for three different  $x$  positions across the plasma column. The direction of the confinement field is such that in this figure counterclockwise rotation corresponds to a mode with left-handed polarization. Indeed this observed polarization is what is expected for a shear Alfvén wave. It should also be noted that the fact that the mode has a local minimum value of the transverse magnetic field at the center of the column (at 32 cm) implies that, for this maser flare near threshold, the azimuthal mode number corresponds to  $m=0$ . The azimuthal structure of the maser is discussed in more detail in Sec. IV.

### C. Behavior well-above maser threshold

Figure 10 shows the temporal evolution of the  $x$  component of the spontaneously excited magnetic field fluctuations (dense dark traces) at a fixed radial position near the center of the main plasma column for a discharge current of 6 kA

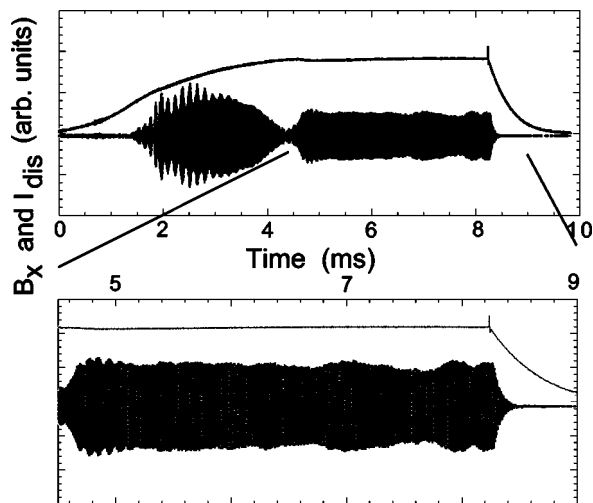


FIG. 10. The temporal behavior of the  $x$  component of the maser field for the 500 G case. Top panel: the discharge current is shown as the top trace, the maser signal is the middle trace. Bottom panel: a blow-up showing the near constant amplitude for more than 3 msec.

and a confinement field of 500 G. These parameters correspond to the far-left region of a horizontal line cutting the current threshold curves of Fig. 8. Physically, this means that the maser action sampled is well above threshold and, accordingly, the amplification is large and robust. The top panel exhibits the behavior sampled over an entire discharge pulse. It shows the development of the maser early in the plasma discharge and it includes an interval  $\approx 3.5$  msec long during which a near steady state is achieved. The thin solid curve shows the time evolution of the discharge current which is terminated, in a controlled fashion, at about the 8.2 msec mark. An expanded view of the steady state is shown in the bottom panel of Fig. 10.

At early times ( $t=2$  msec) an initial burst of maser activity arises as the discharge current grows and then a transition to a near steady-state behavior occurs at about 4.5 msec as the macroscopic discharge parameters also attain a steady state. During the final 3 msec of the pulse, the frequency of the maser fluctuations is constant and the amplitude nearly so. The 3 msec period of constant frequency operation corresponds to 395 wave cycles, yielding a ratio of  $\delta\omega/\omega=5 \times 10^{-3}$ . This example clearly demonstrates that an Alfvén wave maser can attain near steady-state conditions when operated well-above threshold in the absence of external manipulation. This is to be contrasted with the flare activity characteristic of near-threshold behavior exemplified by Fig. 6.

#### IV. MODE TRANSITIONS

In the operation of conventional masers and lasers mode transitions (or “mode hops”) frequently develop and mitigating conditions must be implemented to lock onto the particular mode desired. This becomes increasingly important as the number of modes supported by the resonant cavity increases. In the resonant cavity in this study, the nonuniformity of the confinement magnetic field prevents the development of higher axial modes; in essence this feature provides an axial

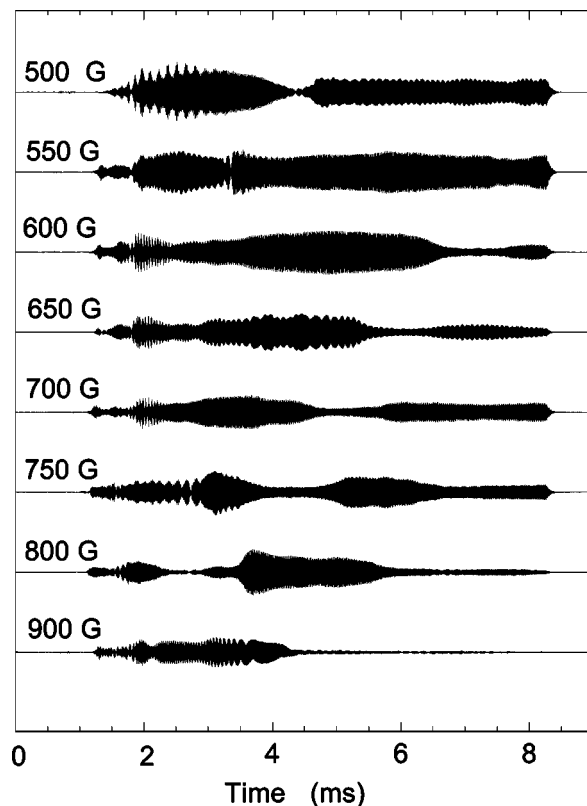


FIG. 11. The temporal signature of the  $x$  component of the maser magnetic field measured in the main plasma column is shown for magnetic fields ranging from 500 to 900 G. The peak discharge current is held constant at 6000 A. The maser reaches near steady state operation for the lower magnetic fields.

mode-locking mechanism. However, no provision is made to restrict the other two degrees of freedom, namely, the radial and azimuthal mode numbers characterizing the global mode structure. It is thus possible for symmetry-breaking features associated with varying plasma parameters to induce mode transitions. These transitions do not alter the two intrinsic features of the maser process, namely, the phase-matching condition in the resonator and the wave-particle resonance. Examples of a variety of spontaneous mode transitions associated with the Alfvén maser are shown in Fig. 11. Each trace corresponds to the temporal evolution of the  $x$  component of the fluctuating magnetic field but displayed on the relatively long time scale ( $\sim 8$  msec) characteristic of the evolution of the plasma discharge. During this long time interval the plasma current (not shown but for all the cases it behaves similarly to that in Fig. 10) rises rapidly in the early portion, reaches a plateau and is shut-off. The various plasma parameters change slowly as the plasma current passes through these phases.

The different traces in Fig. 11 illustrate the dependence of the maser signals on the strength of the confinement magnetic field over the range of 500–900 G for a fixed discharge current of 6 kA. This situation corresponds to traversing a horizontal line from left to right in the threshold curves of Fig. 8, so that the maser action sampled is well-above threshold for the lowest field strength and approaches threshold as the field is increased. For the lowest fields there is an initial

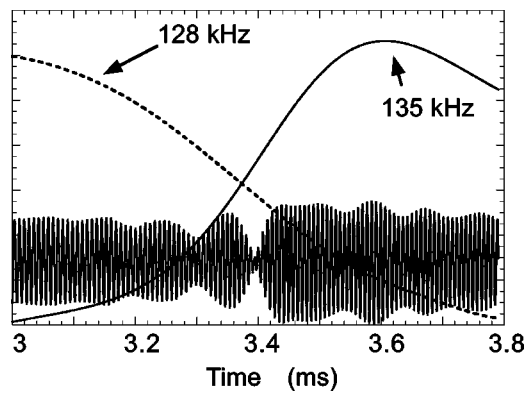


FIG. 12. The maser frequency changes as the plasma discharge current grows. The temporal signal of the maser together with the wavelet amplitude is shown during the frequency transition that occurs during the 550 G case shown in Fig. 11. Two modes of different frequency are present during the transition, producing a visible beat pattern in the maser signal.

burst of maser activity as the discharge current grows and then a transition to a near steady-state behavior as the macroscopic discharge parameters also attain a steady state. Of course, the absolute values of the plasma parameters also experience a change as the magnetic field is varied.

It is seen from Fig. 11 that as the strength of the confinement magnetic field is increased the initial burst and subsequent transition move to earlier times and thus occur at lower plasma current. At 600 G a second transition to lower amplitude occurs at a late time when the discharge current is nearly constant. This second transition is seen to occur at earlier times as the strength of the confinement field is increased. At 800 G the maser amplitude is very small late in the discharge when the discharge current is largest, and at 900 G the maser activity is confined to early times when the discharge current is increasing.

The transition between bursts of maser activity seen in Fig. 11 corresponds to changes in the mode frequency, as is suggested by the “beat pattern” that accompanies the transitions. To illustrate this “frequency evolution” a wavelet analysis of the time series is implemented for the 550 G case and the result is displayed in Fig. 12. It is seen that the amplitude of the first excited mode at 128 kHz decreases while the amplitude at 135 kHz increases until it is the only mode present. For an interval of time both modes coexist and thus give rise to a beat pattern in the time series with an amplitude modulation at the difference frequency. For at least a millisecond before the transition (at 3.4 msec) the 128 kHz mode is the only one present, while after the transition the 135 kHz mode is sustained up to the controlled termination of the discharge.

The mode transition occurs while the density profile across the confinement magnetic field is evolving towards its final steady state. However, the time-scale for the mode transition shown in Fig. 12 is much shorter than that for significant density rearrangement. An example of the two different density profiles sampled by the early mode at 128 kHz and by the steady-state signal at 135 kHz is shown in Fig. 13. The curves correspond to ion saturation current measurements along the horizontal  $x$  position at an axial position  $z$

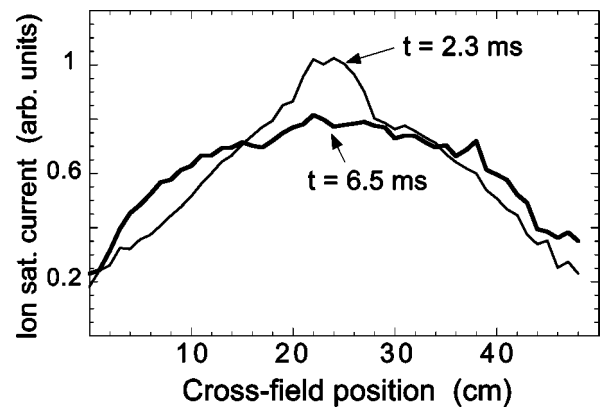


FIG. 13. The density profile of the plasma column changes as the discharge current grows. At early times ( $t=2.3$  msec) the ion saturation current radial profile is narrow and peaked, while at later times ( $t=6.5$  msec), during steady state conditions, it is broad and flat.

$=5.85$  m from the cathode. The curves shown correspond to an ensemble average over ten similar discharges at each position. It is seen that at early times ( $t=2.3$  msec) there is a steep, core feature  $\approx 8$  cm wide that connects to a nearly linear decrease having a much larger scale length. The late-time profile ( $t=6.5$  msec) is characteristic of the steady state. It no longer displays the steep core feature and exhibits a relatively flat spatial dependence that results in an effectively broader profile than is seen at early times.

It is observed that the transition in mode frequency is accompanied by a change in the mode eigenfunction, as is illustrated in Fig. 14 which displays data obtained at an axial field strength of 600 G. The maser at this field strength shows a frequency transition similar to the 550 G case, but the shift is from 140 to 148 kHz. The left side of the figure

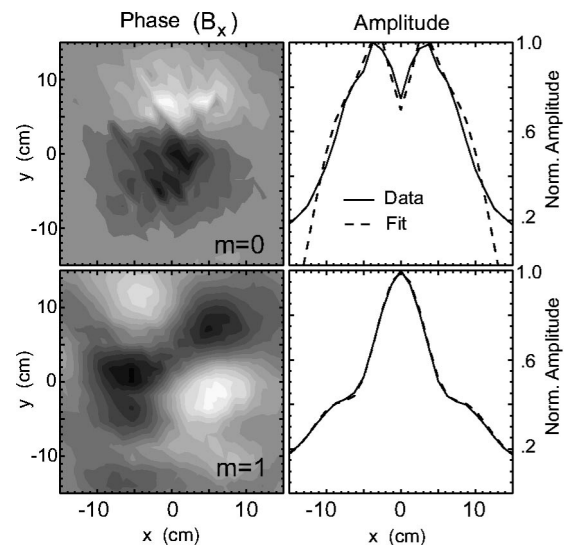


FIG. 14. The maser changes mode structure and the frequency changes as the plasma column evolves. The left hand panels show the cross covariance of the  $x$  components of the wave magnetic fields at an early time (top) when the azimuthal mode number  $m=0$ , and a late time during steady-state conditions (bottom) when  $m=1$ . The right hand panels show radial profiles of the fluctuation amplitude (solid curves) compared to a model Bessel function fit (dashed curves).

displays the cross covariance of the  $x$  component (i.e., horizontal component) of the magnetic field fluctuations associated with the maser. This data is obtained by mixing the signal measured by a movable probe at  $z=7.05$  m that scans across the confinement magnetic field (i.e., in the  $x$ - $y$  plane) with that of a fixed reference  $B$ -dot probe at axial location  $z=7.95$  m. The top left panel shows the pattern of the early 140 kHz signal while that for the late 148 kHz mode is given in the left bottom panel. From these patterns it is found that the early mode exhibits an eigenfunction characterized by an azimuthal mode number  $m=0$ , while the higher-frequency mode corresponds to mode number  $m=1$ . The panels on the right-side display the horizontal variation (i.e., a line cut along the  $x$  direction) of the amplitude of the magnetic fluctuations corresponding to the patterns shown on the left-side panels. The cylindrical symmetry of the LAPD suggests that the radial eigenmode profiles could be fit using Bessel functions.

In a cylindrical plasma column, the azimuthal component of the shear mode magnetic field is expected to be proportional to  $J'_m(k_r r) \exp(im\phi)$ , where prime denotes the derivative of the Bessel function with respect to argument.<sup>23</sup> Hence  $m=0$  is proportional to  $J_1(k_r r)$  and  $m=1$  is proportional to  $J_0(k_r r) - J_2(k_r r)/k_r r$ . Therefore, the  $m=0$  mode has a local minimum near the center of the plasma, while the  $m=1$  mode has a local maximum. This behavior may be understood by considering the currents associated with each mode. The  $m=0$  mode has a single current channel on axis, which produces a field pattern with a minimum on axis. The  $m=1$  mode has two opposing off-axis current channels which give rise to a field maximum between the two channels.

The solid curve corresponds to the measurements while the dashed curve is a numerical fit consisting of the sum of two Bessel functions having different radial scales. The fits are sampled along a line,  $y=1.5$  cm, above the center of cylindrical symmetry, as is suggested by the weak null sampled in the data. It is seen from the relatively good agreement provided by the Bessel-function fit that the maser eigenfunction locally adjusts to accommodate the different length scales of the density profile and of the free-energy source profile (not measured).

From the functional dependence of the fitting curves it is deduced that the dominant radial wave number of the early 140 kHz mode is  $k_r=(2.4/6)$  rad/cm while that for the 148 kHz mode is  $k_r=(3.8/6)$  rad/cm. The 2.4 and 3.8 factors arising, of course, from the zeros of the  $J_1$  and  $J_0$  Bessel functions associated with the  $m=0$  and  $m=1$  behaviors. From this comparison it can be deduced that the contribution to the eigenfrequency, arising from the change in transverse wave number [i.e.,  $(k_\perp \rho_s)^2$ ] in Eq. (1), results in a fractional increase in frequency approximately given by  $2\Delta f/f \approx [(3.8/6)^2 - (2.4/6)^2] / [1 + (2.4/6)^2] = 0.2$ , for a nominal value of  $\rho_s=1$  cm. This is to be contrasted to the observed increase during the mode transition to  $2\Delta f/f=2(8/140)=0.11$ . Given the uncertainty in the evaluation of  $\rho_s$  and of the effective  $k_r$  of the maser eigenfunctions, it can be concluded that the frequency increase associated with the mode transition is consistent with an increase in radial wave num-

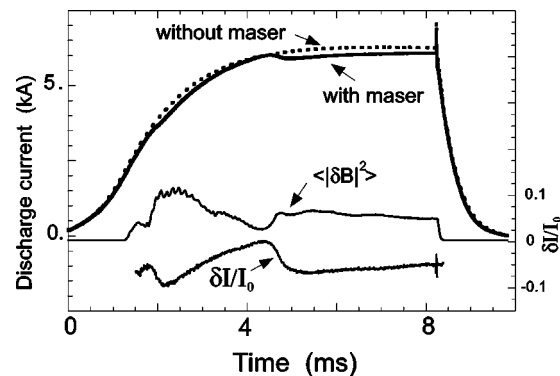


FIG. 15. The maser magnetic field is large enough to effect the discharge current. The discharge current with no maser present at 1300 G (dotted curve) is compared to the discharge current at 550 G (solid curve) when the maser is active. The column average square of the magnetic field amplitude ( $\langle |\delta B|^2 \rangle$ ) and the normalized difference of the two discharge current traces ( $\delta I/I_0$ ) are also shown.

ber. Much more detailed measurements and theoretical developments are required to arrive at a closer quantitative test.

## V. NONLINEAR EFFECTS

The amplitude attained by the magnetic fluctuations arising from maser action can be relatively large, i.e.,  $\delta B/B_0 \approx 1.5\%$ . This level is larger than the square root of the electron to ion mass ratio  $(m/M)^{1/2}$  which is a reasonable indicator of when the properties of shear Alfvén waves become significantly modified by nonlinear processes. The nonlinearities can manifest as a distortion of the wave forms and/or modification of the ambient plasma parameters, in particular, those parameters that are responsible for providing the amplification of the signals. This section briefly presents examples of these features to complete the description of maser action, but these complex processes require a separate and more detailed study.

It is found that the maser activity modifies the discharge current. The thick solid curve in Fig. 15 compares the time evolution of the discharge current for the 500 G case (corresponding to the maser well-above threshold), to a reference discharge current at 1300 G (dotted curve) where the same current is below threshold and there is no maser activity. Also shown for reference in Fig. 15 is the square of the perpendicular component of the maser magnetic field averaged across the plasma column  $\langle |\delta B|^2 \rangle$  together with the difference between the discharge current, with and without the maser present, normalized to the discharge current at 1300 G,  $\delta I/I_0$ . When the maser action is present, the discharge current tends to be below the value without the maser fluctuations, as if an effective resistance is added to the external discharge circuit. This effective resistance is found to be nearly proportional to the square of the maser fluctuations. As the confinement magnetic field  $B_0$  is increased the relative change in the discharge current decreases, even though the peak of the column-averaged maser field energy density relative to the background field energy density (i.e.,

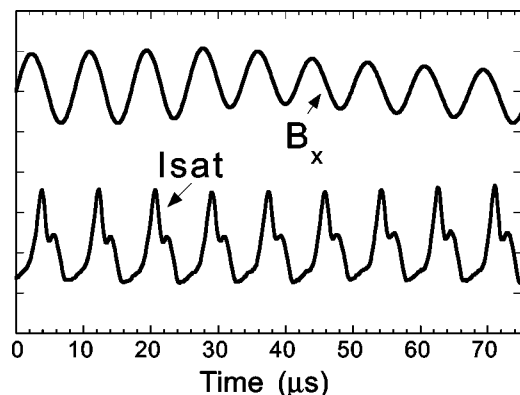


FIG. 16. Ion saturation current obtained in the source region (bottom curve) is compared to the magnetic field (top curve) measured in the main plasma column when the maser is active. The ion saturation current exhibits nonlinear distortions while the magnetic field signal does not.

$\langle(|\delta B|/B_0)^2\rangle$ , remains nearly constant. In addition, as seen in Fig. 11 the time interval over which the maser is active decreases as  $B_0$  is increased.

The effective resistance accompanying maser action has an intrinsic component resulting from the radiation resistance, i.e., from the integrated Poynting flux emanating from the cathode-anode region into the uniform plasma column. This effect contributes a decrease in discharge current, at fixed voltage  $V_0$ , given by  $\delta I = f\lambda a^2 \langle|\delta B|^2\rangle / (4V_0)$  with  $f\lambda$  given by Eq. (1) and  $a$  is the effective radius of the radiation pattern. For characteristic operational parameters this current decrease is on the order of a few-hundred amperes which can account for almost all of the change seen in Fig. 15. The remaining contribution must then be a result of microscopic processes, but the present resolution in the measurements does not permit a quantitative determination of this effect.

Figure 16 illustrates the temporal patterns observed during intense maser action. The top trace corresponds to the  $x$  component of the magnetic fluctuations at an axial position within the uniform column while the bottom trace is the ion saturation current measured simultaneously at a location within the cathode-anode region. It is seen that, indeed, the activity in the resonator cavity and in the free-propagating region are phase correlated. However, the propagating magnetic wave form does not experience a significant temporal distortion but the ion saturation current does. The lack of harmonic distortion in the magnetic signal is expected because the harmonic components are above the ion cyclotron frequency and are thus very small because these frequencies do not correspond to propagating signals. The strong distortion in the ion saturation current can arise from electron temperature changes, density modifications and changes in the fast electron distribution function, all of which need not be associated with propagating signals.

## VI. CONCLUSIONS

This study demonstrates that a steady-state Alfvén wave maser can be realized in the laboratory under controlled conditions. The configuration shares the essential elements of lasers and maser devices that operate at optical and micro-

wave frequencies, namely, a resonant cavity with a partially reflecting boundary and an active medium that provides amplification. Because of the peculiar properties of shear Alfvén waves, these elements take a form different from the optical cavities and inverted atomic populations typically found in conventional lasers and masers. The resonant cavity used here consists of a cathode and a semitransparent mesh anode that permits the amplified shear Alfvén waves to propagate into a large plasma column. In this region, where the magnetic field is uniform, the unique properties of the maser signal can be exploited to study a wide variety of interactions of relevance to magnetic confinement research and space plasma investigations. The generic concept of Alfvén wave masers was first introduced in theoretical studies of near-earth plasmas to explain the properties of spontaneous magnetic fluctuations observed by spacecraft and ground-based detectors. The specific realization of this idea in the laboratory enhances the credibility of the fundamental concept and suggests that there may be a wide variety of configurations that result in Alfvén maser action. Some of these may have relevance to magnetized objects of astrophysical interest.

The Alfvén maser produces a highly coherent shear mode with  $\delta\omega/\omega \approx 5 \times 10^{-3}$  excited spontaneously from ambient noise when a threshold plasma current is exceeded. There is no need for external pumping to trigger the maser action. The amplitude of the magnetic fluctuations associated with the noise-grown signal attains a level exceeding 1.5% of the confinement magnetic field. The frequency of the maser mode is continuously tunable by changing the strength of the confinement field. Its specific value is determined by the cathode-anode separation and the dispersion relation of the shear mode. For the particular experimental arrangement in the LAPD this corresponds to  $\omega = 0.6\Omega_{ci}$ .

A quantitative comparison of the measured threshold plasma current, over a factor of 2 variation in confinement field, shows that the amplification mechanism is the electron drift velocity associated with the natural return current in the plasma. From the best data fits it is deduced that the effective radius associated with the return current is narrow compared to the radial dimension of the plasma column.

The nonuniform magnetic field in the resonant cavity plays an important role in limiting the number of maser modes because shear Alfvén waves do not propagate for frequencies larger than the local value of ion cyclotron frequency. The lower effective magnetic field within the resonant cavity also lowers the speed of propagation of the maser signal which, in turn, results in a smaller threshold plasma current.

The maser action exhibits a wide range of temporal variability. Near threshold it consists of flare events whose statistics displays a non-Gaussian tail. For conditions well-above threshold the maser behavior reaches a steady state whose duration is determined by the lifetime of the plasma discharge. Mode transitions, from azimuthal mode number  $m=0$  to  $m=1$ , occur and are associated with slow changes in the radial density profile and with changes in plasma parameters. During a finite time interval both modes coexist and give rise to characteristic beat patterns. Small drifts in the

frequency of a single maser mode also result from slowly evolving plasma parameters.

Under steady-state conditions the radiation resistance associated with the Poynting flux emanating from the resonant cavity modifies the discharge current. In spite of the relatively large level of the signals, the related magnetic fluctuations do not exhibit a significant nonlinear distortion. This may be expected because, at the maser frequency of  $0.6\Omega_{ci}$ , the higher-harmonic modes are nonpropagating. However, ion saturation signals, that are phase coherent with the maser fluctuations, indeed exhibit strong nonlinearity.

In summary, it has been demonstrated that Alfvén wave masers can be realized in the laboratory. The maser is not only a useful laboratory tool for investigating a wide variety of problems related to Alfvénic interactions, but may also be an important process in space and astrophysical plasmas.

### ACKNOWLEDGMENTS

The work of J.E.M. and G.J.M. was sponsored by NSF Grant No. 0013151000 and that of T.A.C. by DOE Grant No. DE-FG03-02ER54688.

<sup>1</sup>S. V. Polyakov, V. O. Rapoport, and V. Yu. Trakhtengerts, *Fiz. Plazmy* **9**, 371 (1983).

<sup>2</sup>P. P. Belyaev, S. V. Polyakov, V. O. Rapoport, and V. Yu. Trakhtengerts, *Geomagn. Aeron.* **24**, 2 (1984).

<sup>3</sup>P. P. Belyaev, S. V. Polyakov, V. O. Rapoport, and V. Yu. Trakhtengerts, *Izv. Vyssh. Uchebn. Zaved., Radiofiz.* **33**, 408 (1990).

<sup>4</sup>V. Yu. Trakhtengerts and A. Ya. Feldstein, *J. Geophys. Res.* **96**, 19363 (1991).

<sup>5</sup>B. J. Thompson and R. L. Lysak, *J. Geophys. Res.* **101**, 5359 (1996).

<sup>6</sup>R. L. Lysak, *J. Geophys. Res.* **104**, 10017 (1999).

<sup>7</sup>O. A. Pokhotelov, D. Pokhotelov, A. Streltsov, V. Khrushev, and M. Parrot, *J. Geophys. Res.* **105**, 7737 (2000).

<sup>8</sup>M. Grzesiak, *Geophys. Res. Lett.* **27**, 923 (2000).

<sup>9</sup>N. Ivchenko, G. Marklund, K. Lynch, D. Pietrowski, R. Torbert, F. Primdahl, and A. Ranta, *Geophys. Res. Lett.* **26**, 3365 (1999).

<sup>10</sup>P. P. Belyaev, T. Bosinge, S. V. Isaev, and J. Kangas, *J. Geophys. Res.* **104**, 4305 (1999).

<sup>11</sup>F. Z. Feygin, A. K. Nekrasov, K. Mursula, J. Kangas, and T. Pikkarainen, *Ann. Geophys.* **12**, 147 (1994).

<sup>12</sup>C. C. Chaston, J. W. Bonnell, C. W. Carlson, J. P. McFadden, R. E. Ergun, R. J. Strangeway, and E. J. Lund, *J. Geophys. Res.* **109**, A04205 (2004).

<sup>13</sup>R. L. Lysak and Y. Song, *J. Geophys. Res.* **107**, 1160 (2002).

<sup>14</sup>N. G. Lekhtinen, G. A. Markov, and S. M. Fainstein, *Izv. Vyssh. Uchebn. Zaved., Radiofiz.* **38** 312 (1995).

<sup>15</sup>H. Fukunishi, Y. Takahashi, M. Sato, A. Shone, M. Fujito, and Y. Watanabe, *Geophys. Res. Lett.* **24**, 2973 (1997).

<sup>16</sup>A. I. Sukhorukov and P. Stubbe, *Geophys. Res. Lett.* **24**, 829 (1997).

<sup>17</sup>V. Yu. Trakhtengerts, *Geomagn. Aeron.* **29**, 3 (1989).

<sup>18</sup>J. E. Maggs and G. J. Morales, *Phys. Rev. Lett.* **91**, 035004 (2003).

<sup>19</sup>R. Boswell, *Nature (London)* **425**, 352 (2003).

<sup>20</sup>J. E. Maggs and G. J. Morales, *Phys. Plasmas* **10**, 2267 (2003).

<sup>21</sup>M. Opher, G. J. Morales, and J.-N. Leboeuf, *Phys. Rev. E* **66**, 016407 (2002).

<sup>22</sup>Y. Amagishi and M. Tanaka, *Phys. Rev. Lett.* **71**, 360 (1993).

<sup>23</sup>L. C. Woods, *J. Fluid Mech.* **13**, 570 (1962).